

## Metal-Organic Frameworks as Drug Delivery Platforms for Ocular Therapeutics

Jesus Gandara-Loe, Isabel Ortuño-Lizarán, Laura Fernández-Sanchez, Jorge L Alio, Nicolas Cuenca, Alfredo Vega Estrada, and Joaquin Silvestre-Albero

*ACS Appl. Mater. Interfaces*, **Just Accepted Manuscript** • DOI: 10.1021/acsami.8b20222 • Publication Date (Web): 18 Dec 2018

Downloaded from <http://pubs.acs.org> on December 18, 2018

### Just Accepted

“Just Accepted” manuscripts have been peer-reviewed and accepted for publication. They are posted online prior to technical editing, formatting for publication and author proofing. The American Chemical Society provides “Just Accepted” as a service to the research community to expedite the dissemination of scientific material as soon as possible after acceptance. “Just Accepted” manuscripts appear in full in PDF format accompanied by an HTML abstract. “Just Accepted” manuscripts have been fully peer reviewed, but should not be considered the official version of record. They are citable by the Digital Object Identifier (DOI®). “Just Accepted” is an optional service offered to authors. Therefore, the “Just Accepted” Web site may not include all articles that will be published in the journal. After a manuscript is technically edited and formatted, it will be removed from the “Just Accepted” Web site and published as an ASAP article. Note that technical editing may introduce minor changes to the manuscript text and/or graphics which could affect content, and all legal disclaimers and ethical guidelines that apply to the journal pertain. ACS cannot be held responsible for errors or consequences arising from the use of information contained in these “Just Accepted” manuscripts.



# Metal-Organic Frameworks as Drug Delivery Platforms for Ocular Therapeutics

*Jesús Gandara-Loe,<sup>a</sup> Isabel Ortuño-Lizarán,<sup>b</sup> Laura Fernández-Sánchez,<sup>c</sup> Jorge L. Alió,<sup>d</sup>*

*Nicolás Cuenca,<sup>b</sup> Alfredo Vega-Estrada,<sup>d</sup> and Joaquín Silvestre-Albero<sup>a,\*</sup>*

<sup>a</sup>Laboratorio de Materiales Avanzados, Departamento de Química Inorgánica-IUMA,  
Universidad de Alicante, E-03690 San Vicente del Raspeig, Spain

<sup>b</sup>Departamento de Fisiología, Genética y Microbiología, Universidad de Alicante, E-03690 San  
Vicente del Raspeig, Spain

<sup>c</sup>Departamento de Óptica, Farmacología y Anatomía, Universidad de Alicante, E-03690 San  
Vicente del Raspeig, Spain

<sup>d</sup>Research and Development Department, VISSUM Corporation, E-03016 Alicante, Spain

**KEYWORDS:** MOFs, Amorphization, Glaucoma treatment, Drug delivery, Ocular therapeutics

## ABSTRACT

Metal-organic frameworks (MOFs) have been evaluated as potential nanocarriers for intra-ocular incorporation of brimonidine tartrate to treat chronic glaucoma. Experimental results show that UiO-67 and MIL-100 (Fe) exhibit the highest loading capacity with values up to 50-60 wt.%, while the performance is quite limited for MOFs with narrow cavities (below 0.8 nm, e.g. UiO-66 and HKUST-1). The large loading capacity in UiO-67 is accompanied by an irreversible structural amorphization in aqueous and physiological media that promotes extended release kinetics above 12 days. Compared to the traditional drawbacks associated with the sudden release of the commercial drugs (e.g., ALPHAGAN), these results anticipate UiO-67 as a potential nanocarrier for drug delivery in intra-ocular therapeutics. These promising results are further supported by cytotoxicity tests using retinal photoreceptor cells (661W). Toxicity of these structures (including the metal nodes and organic ligands) for retinal cells is rather low for all samples evaluated, except for HKUST-1.

## 1. INTRODUCTION

Glaucoma is the second leading cause of irreversible blindness worldwide with millions of people, aged 40 and older, affected by its common form, open-angle glaucoma.<sup>1</sup> After an initial diagnosis, medication is the main treatment nowadays to halt further loss of vision. Glaucoma is a multifactorial disease, usually associated to an increased pressure within the eye, and the associated damage in the optical nerve, resulting in vision impairment and even blindness. Among the different drugs available in the market, brimonidine is one of the most widely applied.<sup>2</sup> Brimonidine is an alpha adrenergic receptor agonist that, upon topical administration, can reduce intraocular pressure (IOP) by reducing aqueous humour production and increasing

1  
2  
3 uveoscleral outflow. Recent studies have shown that brimonidine has no adverse effects on  
4  
5 different retinal cells, but rather it shows neuroprotective effects on retinal ganglion cell  
6  
7 degeneration in glaucoma.<sup>3,4</sup> In fact, these and other results together with clinical trials have  
8  
9 derived in the commercialization of brimonidine for the treatment of glaucoma under European  
10  
11 medication agency (EMA) mandate (REF: EMA/366180/2017). Despite the high benefits of the  
12  
13 drug, topical administration is usually associated with important drawbacks such as poor  
14  
15 bioavailability (only 5% of the administered drug reaches the interior of the eye), side effects due  
16  
17 to rapid drainage through nasolacrimal duct, and the necessity for multiple administration (2-3  
18  
19 eye drops daily for many years). Taking into account the low compliance of patients to strictly  
20  
21 follow the treatment and the detrimental effects in case of breach, new therapies are required to  
22  
23 improve the quality of life in patients and to decrease their dependence on external medication.  
24  
25  
26  
27

28  
29 One of the most promising alternatives for a long-term treatment of glaucoma consist in the  
30  
31 incorporation of the drug in platforms or vehicles able to concentrate the drug and release it at  
32  
33 the target in a controlled way, increasing the bioavailability and avoiding the traditional “burst  
34  
35 effects”. These delivery systems include hydrogels<sup>5</sup>, microspheres<sup>6</sup>, nano-vesicles<sup>7</sup>,  
36  
37 nanoparticles<sup>8</sup>, microfilms<sup>9</sup>, among others. Unfortunately, these formulations based on  
38  
39 macromolecules or polymers suffer from low loading capacity (gravimetric < 1 wt. % and/or  
40  
41 volumetric <0.1 wt./vol. %) and fast release of the drug (within minutes/hours).<sup>10-12</sup> These  
42  
43 numbers can be improved through the incorporation of denser inorganic matrices in the  
44  
45 formulation, for instance montmorillonite clay and layered double hydroxides (LDH).<sup>13,14</sup>  
46  
47 Montmorillonite/chitosan nanoparticles have been evaluated as delivery systems for betaxolol  
48  
49 hydrochloride, a selective beta-adrenergic blocking agent, with excellent values of drug loading  
50  
51 capacity (up to 14.5 wt.%) and delivery kinetics between 6-10h.<sup>13</sup> Sun et al. reported the  
52  
53  
54  
55  
56  
57  
58  
59  
60

1  
2  
3 synthesis of composites using a thermogel incorporated with brimonidine-loaded LDH  
4 nanoparticles with a significant loading capacity (up to 0.125 mg/g), although lower than the  
5 original LDH (25.0 mg/g or 2.5%), and an improved release profile (up to 2 days are required to  
6 release 75%) compared to the original LDH.<sup>14</sup> These studies mainly focused in pre-corneal  
7 administration, thus keeping the concerns about bioavailability in the interior of the eye (low  
8 penetration of the drug through the cornea; < 1-7%).  
9

10  
11 Taking into account the limited volume of the ocular cavity (< 3-4 cm<sup>3</sup>) and the limited  
12 allowance of fluid (human eye can hold only 7-10 µl of fluid), any intraocular delivery platform  
13 for ocular therapeutics needs to fulfil even more stringent requirements compared to pre-corneal  
14 devices such as i) extremely large loading capacity (in gravimetric (wt.%) and volumetric (w/v  
15 %) basis) to mitigate any interference in the visual field after dosing, ii) slow delivery kinetics  
16 (within days or weeks) to allow long-term therapy, iii) high biocompatibility for retinal cells and,  
17 last but not least, iv) structural instability once the material has completed the job.  
18

19  
20 Potential candidates able to fulfil these requirements are metal-organic frameworks (MOFs).  
21 The proper combination of metallic nodes or clusters and organic ligands allows to design a wide  
22 variety of 1-3D networks characterized by an extremely large surface area and pore volume.<sup>15</sup>  
23 Previous studies described in the literature have shown that MOFs are potential candidates for  
24 drug delivery with excellent results for a wide variety of drugs such as antitumoral, retroviral,  
25 etc.<sup>16,17</sup> Furthermore, *in vitro* and *in vivo* cytotoxicity assays have anticipated a promising  
26 performance with low toxicity and inflammatory activity.<sup>16-18</sup> To our knowledge, MOFs have  
27 never been tested as potential drug delivery platforms for ocular therapeutics.  
28

29  
30 Based on these premises, the main goal of the present study is the evaluation of several MOFs  
31 in the adsorption and release of brimonidine for glaucoma treatment, the evaluation of their  
32

1  
2  
3 structural stability in the charging/discharging media and, last but not least, the evaluation of the  
4 cytotoxicity of the different components (bulk MOF, linker and metallic precursors) in retinal  
5 photoreceptor culture cells (661W).  
6  
7  
8  
9

## 10 11 12 **2. EXPERIMENTAL SECTION** 13

### 14 15 **2.1. Synthesis and characterization of MOFs** 16

17  
18 UiO-66, UiO-67 and MIL-100(Fe) MOFs have been synthesized based in previous works  
19 reported in the literature. UiO-66 and UiO-67 were synthesized based in the procedure reported  
20 by Katz et al.<sup>19</sup> For UiO-66, 0.5 g of ZrCl<sub>4</sub> were dissolved in 20 mL of DMF and 4 mL of  
21 concentrated HCl. In a second vessel, 0.492 g of terephthalic acid (BDC) were dissolved in 40  
22 mL of DMF. The two solutions were mixed and maintain under stirring for 30 min. The  
23 transparent final solution was transferred to a 200 mL jar, closed tightly and kept at 353 K  
24 overnight. The synthesis procedure for UiO-67 was similar to the one described for UiO-66.  
25 Briefly, 0.360 g of 4,4'-biphenyldicarboxylic acid (BDPC) were added to a mixture of 20/2 mL  
26 of DMF/concentrated HCl and 0.268 g of ZrCl<sub>4</sub> were dissolved into 40 mL of DMF. The two  
27 solutions were mixed and stirred for 30 min. The white coloured final solution was placed into a  
28 200 mL jar, closed tightly and kept at 353 K overnight. The resulting solid was filtered and  
29 washed first with DMF (2x30 mL) and then with ethanol (2x30 mL). Samples were activated  
30 under low vacuum ( $13 \cdot 10^3$  Pa) until a temperature of 363 K was reached. The samples were then  
31 subjected to an outgassing treatment at 423 K for 3 h under ultra-high vacuum conditions. MIL-  
32 100 (Fe) was prepared using the facile low temperature synthesis procedure reported in the  
33 literature by Zhang et al.<sup>20</sup> Briefly, 4.04 g of Fe(NO<sub>3</sub>)<sub>3</sub>·9H<sub>2</sub>O and 1.89 g of trimesic acid  
34 (H<sub>3</sub>BTC) were dissolved in 6 mL of distillate water and kept under reflux at 368 K overnight.  
35  
36  
37  
38  
39  
40  
41  
42  
43  
44  
45  
46  
47  
48  
49  
50  
51  
52  
53  
54  
55  
56  
57  
58  
59  
60

1  
2  
3 The solid was purified three times using a solvent extraction treatment with deionized water (350  
4 ml) and ethanol (350 ml) at 343 K for 24 h, and finally dried in vacuum at 423 K for 10 h.  
5  
6  
7 HKUST-1 (Cu) has been used as received from the Sigma-Aldrich, labelled and commercialize  
8  
9 as Basolite C 300.  
10

11  
12 X-ray diffraction patterns of the samples were recorded using a Bruker D8-Advance equipment  
13  
14 with mirror Goebel with high temperature Chamber and a generator of X-ray  
15 KRISTALLOFLEX K 760-80F with a tube of RX with copper anode. Spectra were registered  
16  
17 between 3 and 80° (2 $\theta$ ) with a step of 0.05° and a time per step of 3 s.  
18  
19

20  
21 Textural properties of the samples were evaluated by gas physisorption of nitrogen at 77 K.  
22  
23 Gas adsorption measurements were performed in a homemade fully automated manometric  
24  
25 equipment designed and constructed by the Advanced Materials Group (LMA), now  
26  
27 commercialized as N2GSorb-6 (Gas to Materials Technologies; [www.g2mtech.com](http://www.g2mtech.com)). The  
28  
29 samples were previously degassed for 8 h at 423 K under vacuum (10<sup>-3</sup> Pa). Nitrogen adsorption  
30  
31 data were used to determine: (i) the total pore volume ( $V_t$ ) at a relative pressure of 0.95, (ii) the  
32  
33 BET specific surface area ( $S_{BET}$ ) and (iii) the micropore volume ( $V_{N_2}$ ) by application of Dubinin-  
34  
35 Radushkevich equation. The difference between  $V_t$  and  $V_{N_2}$  is considered to be the mesopore  
36  
37 volume ( $V_{meso}$ ).  
38  
39  
40

41  
42 The size and shape of the synthesized crystals was evaluated using field emission scanning  
43  
44 electron microscopy (FESEM). These analyses were performed in a Merlin VP Compact system  
45  
46 from ZEISS with a resolution of 0.8 nm at 15 kV and 1.6 nm at 1 kV. FTIR spectra were  
47  
48 recorded on a JASCO FTIR 4700 spectrometer with a resolution of 2 cm<sup>-1</sup>.  
49  
50

51  
52 Structural stability of the MOFs was evaluated by immersing 0.1 g of each MOF in 50 mL of  
53  
54 an aqueous solution or a phosphate-based solution (PBS) for 1h, 1 day, 7 days and 30 days. After  
55  
56  
57  
58  
59  
60

1  
2  
3 this time intervals, the material was washed with ultrapure water and filtered in vacuum. After an  
4  
5 evacuation at 393 K for 8 h, the crystallinity of the materials was checked using XRD analysis.  
6  
7  
8  
9

## 10 **2.2. Loading and release experiments**

11  
12 Brimonidine tartrate quantification was done based on the spectrometric method developed by  
13  
14 Bhagav et al.<sup>21</sup> A 1500 ppm stock solution of brimonidine tartrate was prepared dissolving 1.5 g  
15  
16 of brimonidine tartrate in 1000 mL of ultrapure water. The calibration curve was constructed  
17  
18 measuring concentrations from 2 to 15 ppm using a UV-Vis spectrophotometer (double-beam  
19  
20 spectrophotometer with a photomultiplier tube detector JASCO V-650 UV-VIS) at wavelengths  
21  
22 of  $\lambda_1 = 247$  nm and  $\lambda_2 = 320$  nm. High performance liquid chromatography (HPLC) was used to  
23  
24 certify the precision of the UV-Vis method in brimonidine quantification.<sup>22</sup> Both methods gave  
25  
26 an accuracy above 97%, thus confirming the validity of the UV-vis technique for brimonidine  
27  
28 determination.  
29  
30  
31  
32  
33  
34

### 35 **2.2.1. Brimonidine loading experiments**

36  
37 For the loading tests, a group of aqueous solutions with an initial concentration of 200 ppm,  
38  
39 500 ppm, 750 ppm, 1000 ppm and 1500 ppm of brimonidine tartrate were prepared from the  
40  
41 stock solution. The MOFs samples were outgassed at 423 K overnight prior to the adsorption  
42  
43 measurement. 100 mg of each MOF were placed in contact with 50 mL of each concentration  
44  
45 and left under stirring until equilibrium was reached. Aliquots were taken in different periods of  
46  
47 time in order to evaluate the kinetic behaviour of each MOF. All samples reached complete  
48  
49 equilibrium after 7 h.  
50  
51  
52  
53  
54  
55  
56  
57  
58  
59  
60



1  
2  
3 The quantification of brimonidine tartrate was determined by UV-Vis spectrophotometry  
4 diluting each aliquot 1:100 and using the method described above. A MOF-loaded blank  
5 experiment was measured to determine possible interferences in the UV-vis signal due to the  
6 MOF degradation. However, no interferences were observed at the wavelengths selected for  
7  
8  
9  
10  
11  
12  
13  
14  
15  
16  
17  
18  
19  
20  
21  
22  
23  
24  
25  
26  
27  
28  
29  
30  
31  
32  
33  
34  
35  
36  
37  
38  
39  
40  
41  
42  
43  
44  
45  
46  
47  
48  
49  
50  
51  
52  
53  
54  
55  
56  
57  
58  
59  
60

The quantification of brimonidine tartrate was determined by UV-Vis spectrophotometry diluting each aliquot 1:100 and using the method described above. A MOF-loaded blank experiment was measured to determine possible interferences in the UV-vis signal due to the MOF degradation. However, no interferences were observed at the wavelengths selected for brimonidine for all MOFs evaluated.

### 2.2.2. Brimonidine release experiments

In an initial step the MOFs were loaded by contacting 100 mg of a degassed MOF with 50 mL of a 500 ppm brimonidine tartrate aqueous solution. The system was left under stirring for 7 h to ensure full equilibrium. After this time, the sample was collected by filtration and an aliquot was saved to determine the maximum loading amount. The brimonidine-loaded MOF was washed several times with ultrapure water and dried under vacuum at 333 K for 6 h. The dried brimonidine-loaded MOF was immersed in 50 mL of physiological solution (PBS) and aliquots were taken at different times up to 12 days. Brimonidine determination has been performed in a similar procedure to that described above. All the dilutions (1:100) and calibration curve were measured using PBS as a solvent instead of ultrapure water.

### 2.3. Cytotoxicity tests

661W cell line, derived from mouse retinoblastoma and considered a photoreceptor cell line, was employed in the cytotoxicity tests. To assess MOFs toxicity in retinal cells, 611W cells were incubated with MOFs and MOFs components at different concentrations for 24h or 48h. A death control was also included in each study to be sure that cells die with a noxious stimulus (0.4 mM sodium nitroprusside, SNP; 228710, Sigma-Aldrich, St Louis, MO, USA).

1  
2  
3 First, for cell viability assays at 24h or 48h after adding the MOFs, cells were plated in 96-well  
4 plates at a density of 10000 or 4000 cells per well respectively. They were incubated in  
5 Dulbecco's modified Eagle's medium (DMEM High Glucose; L0106, Biowest, Nuaille, France)  
6 supplemented with 10% fetal bovine serum (FBS; SV30160, GE Healthcare, Pasching, Austria),  
7 1% penicillin/streptomycin (P9781, Sigma-Aldrich) and 1% L-Glutamine (25030-081, Gibco,  
8 Paisley, UK), and maintained during the whole experiment at 310 K in a humidified atmosphere  
9 with 5% CO<sub>2</sub>. 24 h after seeding, medium was replaced and 0.4 mM SNP or MOF concentrations  
10 of 0, 10, 20, 30, 40 and 50 µg/ml in supplemented DMEM were added. Each condition was done  
11 at eight replicates per plate. MOFs and their respective components were maintained in the  
12 medium and cell viability was assessed at 24 and 48 hours using the XTT cell viability assay  
13 (X4626, Sigma-Aldrich). Briefly, this kit consists of a colorimetric assay dependent of a redox  
14 reaction that measures mitochondrial activity and thus is an estimate of cell quantity. 100 µl of  
15 XTT was added to each well, incubated at 310 K and 5% CO<sub>2</sub> for 2 hours and absorbance  
16 measured at 492 nm in a Beckman Coulter AD340 plate reader (Beckman Coulter Inc., Nyon,  
17 Switzerland). Absorbance was transformed into viability percentage considering the value of the  
18 0 µg/ml concentration (positive control) as 100% cell viability. All these procedures were done  
19 in sterile conditions, using sterile materials and solutions, and MOFs were heat-sterilized at 423  
20 K for 3 hours prior to use.

### 21 22 23 24 25 26 27 28 29 30 31 32 33 34 35 36 37 38 39 40 41 42 43 44 45 46 47 **3. RESULTS AND DISCUSSION**

48  
49  
50 Four different MOFs have been selected for this study, i.e. HKUST-1, MIL-100 (Fe), UiO-66  
51 and UiO-67. The main goal is to evaluate systems with a different porous structure (from purely  
52 microporous to micro/mesoporous systems) and different surface chemistry to evaluate the role  
53  
54  
55  
56  
57  
58  
59  
60

1  
2  
3 of these parameters in the loading and delivery performance. Furthermore, these MOFs have  
4 been selected based in the *a priori* low toxicity of the metal species incorporated: zirconium  
5 chloride lethal dose LD<sub>50</sub> ~3500 mg/kg (for UiO-66 and UiO-67), and iron nitrate lethal dose  
6 LD<sub>50</sub> ~3250 mg/kg (for MIL-100(Fe)), except HKUST-1 with a potential toxicity due to the  
7 copper nitrate used (LD<sub>50</sub> ~940 mg/kg).<sup>23</sup> The selection of HKUST-1 is based on the excellent  
8 performance that has been reported in the literature for this material for a wide range of  
9 applications, e.g. methane and hydrogen storage,<sup>24-26</sup> hydrocarbon separation,<sup>27</sup> etc. Briefly,  
10 HKUST-1 is assembled from Cu<sub>2</sub>(H<sub>2</sub>O)<sub>2</sub> dimer units and tridentate trimesate groups to form 3D  
11 channels with alternating cavities of diameter ~1.4 nm and ~1.1 nm connected through pore  
12 windows of ~1.0 nm.<sup>28</sup> There are also smaller diameter cavities of ~0.5 nm between the larger  
13 cavities. MIL-100 (Fe) consist on trimers of metal octahedra and trimesic acid as a linker.<sup>16</sup> This  
14 material possesses cages in the mesoporous range (diameter ~2.5 and ~2.9 nm), accessible  
15 through pore windows of 0.48 x 0.58 nm, for the small cage, and 0.86 nm, for the larger one.  
16 Finally, UiO-66 and UiO-67 are constituted by clusters of Zr<sub>6</sub>O<sub>4</sub>(OH)<sub>4</sub>(CO<sub>2</sub>)<sub>12</sub> connected through  
17 benzene-dicarboxylate and biphenyl-dicarboxylate linkers, respectively. The longer linker in the  
18 last case gives rise to larger tetrahedral and octahedral microporous cages, i.e. 0.75 nm and 1.2  
19 nm, for UiO-66, and 1.2 nm and 1.6 nm, for UiO-67. Figure S1 shows a schematic drawing of  
20 the evaluated MOFs.  
21  
22  
23  
24  
25  
26  
27  
28  
29  
30  
31  
32  
33  
34  
35  
36  
37  
38  
39  
40  
41  
42  
43  
44  
45  
46  
47  
48  
49  
50  
51  
52  
53  
54  
55  
56  
57  
58  
59  
60

**Table 1.** Textural properties of the synthesized MOFs.

Sample	$S_{\text{BET}}$ ( $\text{m}^2/\text{g}$ )	$V_0$ ( $\text{cm}^3/\text{g}$ )	$V_t$ ( $\text{cm}^3/\text{g}$ )
HKUST-1	1690	0.65	0.72
MIL-100 (Fe)	1360	0.42	0.79
UiO-66	1465	0.53	0.69
UiO-67	2620	1.02	1.24

The textural characteristics of the synthesized materials have been evaluated using nitrogen adsorption at cryogenic temperatures. These measurements are mandatory to certify the validity of the synthesis method applied and to confirm the quality of the synthesized nanocrystals. Figure S2 shows the  $\text{N}_2$  adsorption/desorption isotherms at 77 K for the four samples evaluated. The nitrogen adsorption capacity for samples HKUST-1, MIL-100 (Fe) and UiO-66 is rather similar, i.e. around 350-400  $\text{cm}^3/\text{g}$ , although with some differences in the shape of the isotherm (knee at low relative pressures). While it is narrower for HKUST-1 and UiO-66 as corresponds to purely microporous materials, the knee is wider and associated with a significant slope in the mid-pressure region in the specific case of the micro/mesoporous MIL-100 (Fe). Compared to UiO-66, longer linkers in UiO-67 give rise to a two-fold increase in the adsorption capacity up to 800  $\text{cm}^3/\text{g}$ . The presence of larger cages ( $\sim 1.6$  nm) in the case of UiO-67 can be clearly appreciated by a sudden jump in the nitrogen adsorption isotherm at  $p/p_0 \sim 0.2$  (right after the filling of the narrow cages). The textural characteristics obtained after application of the BET and the Dubinin-Radushkevich (DR) equations are collected in Table 1. The reported values are in close agreement with the literature, thus validating the synthesis procedure.

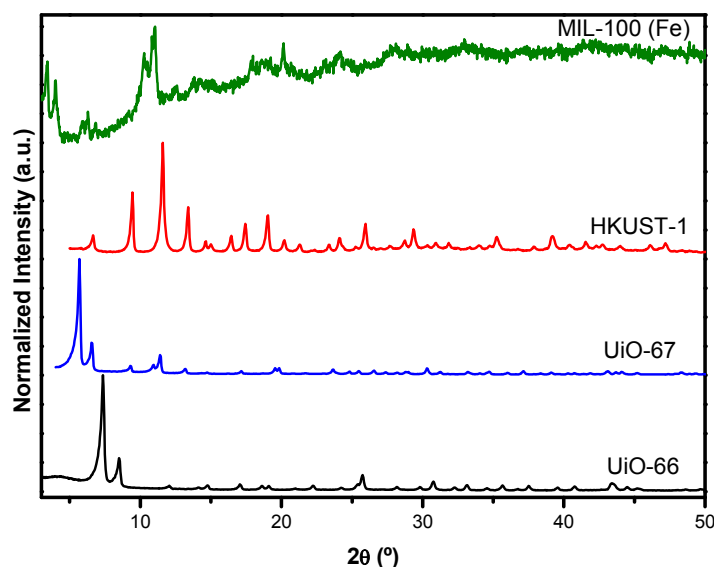


**Figure 1.** X-ray diffraction pattern of the different MOFs evaluated.

In addition to the textural properties, the crystallinity of the synthesized MOFs has been evaluated using X-ray diffraction. Figure 1 shows the XRD pattern for each of the four MOFs evaluated in the  $2\Theta$  range  $2-50^\circ$ . These patterns perfectly match those described in the literature for these materials, thus confirming the quality of the synthesized metal-organic frameworks.

The size and shape of the synthesized nanocrystals have been evaluated using FESEM. The morphology of the synthesized nanocarriers, preferentially the crystal size, is of paramount importance in ophthalmological applications to minimize potential disruption in the visual field upon injection and/or undesired sedimentation in the ocular cavity. Figure S3 shows representative images for the MOFs evaluated. As it can be observed, MIL-100 (Fe), UiO-66 and UiO-67 are constituted by nanometer size crystals (average crystal size  $140 \pm 30$  nm,  $80 \pm 10$  nm and  $120 \pm 20$  nm, respectively). Only HKUST-1 exhibits larger crystals in the micrometer size range (average crystal size  $3 \pm 1$   $\mu\text{m}$ ).

1  
2  
3 Last but not least, the vibrational modes of the synthesized MOFs have been evaluated using  
4 FTIR (Figure S4). FTIR spectra constitute a fingerprint to further certify the quality of the  
5 synthesized MOFs, including the surface functional characteristics. The four samples evaluated  
6 exhibit similar vibrational bands in the 1300-1700  $\text{cm}^{-1}$  range attributed to the structural  
7 carboxylate groups in the linkers.<sup>29</sup> More specifically, the peaks around 1368  $\text{cm}^{-1}$  and 1448  $\text{cm}^{-1}$   
8 corresponds to symmetric stretching vibrations of the carboxylate group (O-C-O groups),  
9 whereas the asymmetric vibrations in the carboxylate appears close to 1550-1650  $\text{cm}^{-1}$ .<sup>30</sup>  
10 Vibration peaks corresponding to the aromatic ring (C=C) are shown at ca. 1500  $\text{cm}^{-1}$ , whereas  
11 bands attributed to the metal cluster and the linkers appear at lower wavenumbers (1000-500  $\text{cm}^{-1}$ ).<sup>31</sup> UiO-66 and UiO-67 exhibit longitudinal and transverse modes of Zr-O vibrations between  
12 660 and 540  $\text{cm}^{-1}$  and the OH and CH bending modes at 770-740  $\text{cm}^{-1}$ . MIL-100(Fe) exhibits  
13 sharp peaks at 760  $\text{cm}^{-1}$  and 709  $\text{cm}^{-1}$  due to the linker bending modes and Fe-O cluster  
14 vibrations, while HKUST-1 shows a band at 727  $\text{cm}^{-1}$  attributed to the Cu-O mode.<sup>32,30</sup> Last but  
15 not least, the absence of significant peaks at 1710-1720  $\text{cm}^{-1}$  attributed to the C=O stretching  
16 vibration of residual trimesic acid suggest the proper purification of the synthesized MOFs.

17  
18  
19  
20  
21  
22  
23  
24  
25  
26  
27  
28  
29  
30  
31  
32  
33  
34  
35  
36  
37  
38 Once the crystallographic structure and morphology of the different MOFs has been validated  
39 and the textural properties confirmed, these materials have been evaluated in the adsorption of  
40 brimonidine tartrate. Liquid phase adsorption isotherms have been quantified at 298 K and at  
41 ranging concentrations using ultra-pure water as charging media. As it can be appreciated in  
42 Figure 2 the amount of drug loaded increases with the concentration of brimonidine in the  
43 aqueous solution, except for HKUST-1 and UiO-66 materials where saturation is already reached  
44 at concentrations above 800 mg/L. Apparently, MOFs with narrow micropores become quickly  
45 saturated, the final loading capacity being around 0.16 g/g. The scenario changes completely for  
46  
47  
48  
49  
50  
51  
52  
53  
54  
55  
56  
57  
58  
59  
60

MOFs with larger micropores/small mesopores such as UiO67 and MIL-100 (Fe). In this specific case, the loading capacity increases with concentration with a loading capacity at 1400 mg/L as high as 0.31 g/g (31 wt.%), for MIL-100 (Fe), and 0.44 g/g (44 wt.%), for UiO-67. Previous studies described in literature for ibuprofen adsorption in MIL-100 (Cr) reported adsorption values around 0.35 g/g, in close agreement with our data.<sup>16</sup> Extrapolation of the adsorption data reported in Figure 2 using the Langmuir equation (dotted line) gives loading values at saturation as high as 0.49 g/g, for MIL-100 (Fe), and 0.63 g/g, for UiO-67. To our knowledge, these are among the best values described in the literature for the adsorption of drugs using metal-organic frameworks.

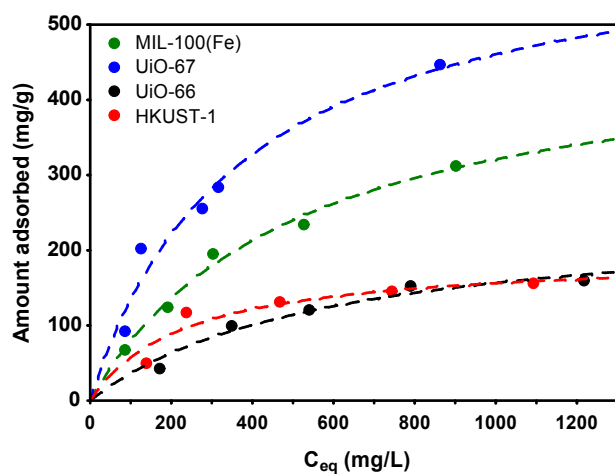


**Figure 2.** Liquid-phase adsorption isotherms for brimonidine tartrate at 298 K. Fitting to Langmuir equation is included (dotted line).

Adsorption results clearly show that UiO-67, with the larger BET surface area and pore volume (above 1 cc/g), is the best performing material over the whole concentration range

1  
2  
3 evaluated with a loading capacity superior to the majority of MOFs reported in the literature so  
4 far for similar drugs. Despite the significant surface area in HKUST-1, this material becomes  
5 saturated immediately with a poor performance at high concentrations. Last but not least,  
6 although MIL-100 (Fe) and UiO-66 exhibit similar textural properties (in terms of BET surface  
7 area and micropore volume), the presence of mesopores in the former MOF play a crucial role  
8 with a loading capacity more than double that of UiO-66. Consequently, these results clearly  
9 anticipate that microporous MOFs with a pore size below 0.8 nm are not appropriate for  
10 brimonidine adsorption due to the limited accessibility of the drug to the interior cavities. This  
11 can also be the reason for the lower loading in MIL-100 (Fe) compared to UiO-67 due to the  
12 limited accessibility of the small cages in the former (pore windows of 0.48 x 0.58 nm). In  
13 addition to the loading capacity, adsorption kinetics are also relevant. As it can be observed in  
14 Figure S5, for an initial concentration of 500 ppm, saturation is reached within 4-5 h, except for  
15 UiO-66 with narrow but accessible cavities with adsorption kinetics slightly above 5h. These  
16 results are very promising since only a few hours are required to load the materials before  
17 injection into the eye.

18  
19  
20  
21  
22  
23  
24  
25  
26  
27  
28  
29  
30  
31  
32  
33  
34  
35  
36  
37  
38 One of the most relevant issues in medical therapies, not frequently addressed in the literature,  
39 concerns the stability of the host structures in the loading and discharging media, i.e. in aqueous  
40 solutions or physiological media (PBS). It is well-known in the literature that several MOFs  
41 exhibit structural deterioration upon exposure to a humid environment.<sup>33, 34</sup> The instability has  
42 been traditionally attributed to the nuclearity, coordination number of the metal, functionality of  
43 linker and framework dimensionality. In our case, we have evaluated the structural stability of  
44 the different MOFs at different time intervals from 1 day until 30 days using an aqueous solution  
45 as a charging media (see Figure S6). At this point it is important to highlight that similar results  
46  
47  
48  
49  
50  
51  
52  
53  
54  
55  
56  
57  
58  
59  
60



1  
2  
3 have been observed in the presence of a physiological solution of PBS as discharging media. As  
4  
5 it can be appreciated, the structural stability highly depends on the nature of the metal-organic  
6  
7 network. While HKUST-1 and UiO-67 exhibit a rapid deterioration in the first 24 hours, samples  
8  
9 UiO-66 and MIL-100 (Fe) remain stable even after 30 days. The irreversible instability of  
10  
11 HKUST-1 is in close agreement with previous findings in the literature in liquid and gas phase.<sup>35</sup>  
12  
13  
14 <sup>36</sup> HKUST-1 suffers degradation due to the strong interaction between the open Cu(II) sites (the  
15  
16 coordinatively unsaturated sites from the copper paddlewheel) and water molecules. This  
17  
18 irreversible instability can explain the low loading capacity for HKUST-1 (see Figure 2), despite  
19  
20 the presence of a significant BET surface area in the as-synthesized material. However, the  
21  
22 presence of limited accessibility for brimonidine to the inner micropores must also be considered  
23  
24 to explain the adsorption results. Contrary to HKUST-1, the results for UiO-67 are more  
25  
26 surprising since this material exhibits the best adsorption performance, despite the drastic  
27  
28 instability observed in the first few hours. To confirm the potential role of brimonidine within the  
29  
30 structure as a stabilizer, we have performed XRD analysis of the loaded material under aqueous  
31  
32 solution right after complete saturation, i.e. after 24h. Figure S7 compares the original XRD  
33  
34 pattern and the ones after 24h in the presence and absence of the drug. As expected, although the  
35  
36 XRD pattern of the loaded MOF already anticipates an important crystallographic deterioration  
37  
38 (amorphization), this damage is lower than the one observed in the absence of the drug, i.e. the  
39  
40 presence of the brimonidine within the structure seems to be crucial to preserve a certain  
41  
42 crystallinity in UiO-67, thus explaining the excellent adsorption results achieved. Upon loading,  
43  
44 the second open question concerns the delivery kinetics. Previous studies described in the  
45  
46 literature for MOFs have shown that 3-5 days release is a common number for this kind of  
47  
48 drugs.<sup>16-18</sup> The main question at this point is the role that instability can exhibit in the release  
49  
50  
51  
52  
53  
54  
55  
56  
57  
58  
59  
60

1  
2  
3 kinetics. Release kinetics were not evaluated for HKUST-1 due to the strong structural  
4 deterioration even in the presence of the drug. Figure 3 shows the amount of brimonidine  
5 released in PBS (discharging media) versus time for the loaded UiO-66, UiO-67 and MIL-100  
6 (Fe) materials (loading performed using a 500 ppm brimonidine aqueous solution). As it can be  
7 observed, all materials exhibit two regimes related to the location of the drug in the structure. An  
8 initial release for 3 days associated with brimonidine weakly bonded within the MOF structure  
9 (ca. 70-80% delivery for MIL-100 (Fe) and UiO-66) and a subsequent slow release of  
10 brimonidine, although quite limited up to 75-85% during next 6-8 days. The absence of complete  
11 release in these two MOFs clearly denotes the presence of brimonidine strongly interacting with  
12 the structural framework. Interestingly, the scenario changes completely in the specific case of  
13 UiO-67. The structural instability in aqueous and PBS media gives rise to an initial release  
14 within 4 days of around 43% and a subsequent and progressive release with time up to a 56%  
15 after 12 days. An extrapolation of these values suggest potentially more than 30 days of  
16 continuous release with the associated benefits for a chronic ocular disorder such as glaucoma.  
17 The beneficial role of the partial amorphization of MOFs in the release kinetics was recently  
18 described by Orellana-Tavra et al. for calcein released in mechanically deteriorated UiO-66.<sup>37</sup>  
19 More than 30 days controlled release could be obtained versus 2 days in the crystalline  
20 counterpart.  
21  
22  
23  
24  
25  
26  
27  
28  
29  
30  
31  
32  
33  
34  
35  
36  
37  
38  
39  
40  
41  
42  
43  
44  
45  
46  
47  
48  
49  
50  
51  
52  
53  
54  
55  
56  
57  
58  
59  
60

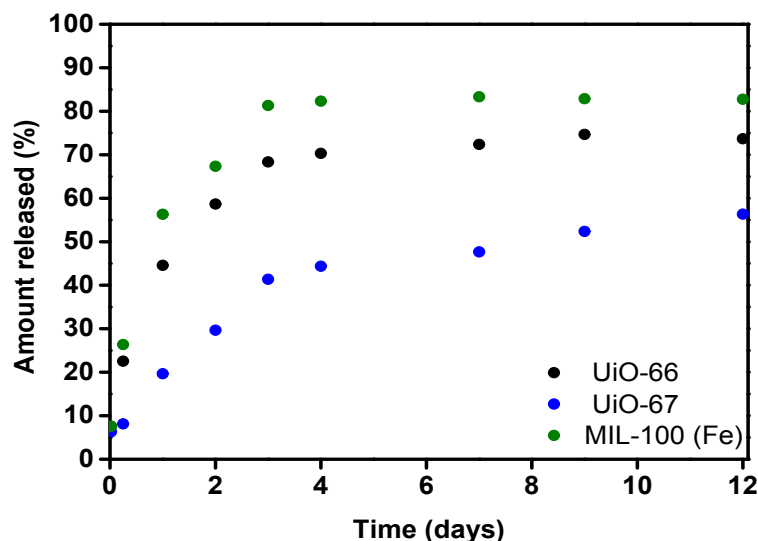


**Figure 3.** Brimonidine tartrate release kinetics at 298 K in physiological media PBS (loading concentration 500 ppm).

As described in the introduction, the final goal of this study is the design of metal-organic frameworks with a high potential to be applied in glaucoma treatment after injection in the intra-ocular cavity. From this perspective, the progressive deterioration of the MOF within the eye while releasing the drug can be anticipated as an optimum performance to promote the complete clearance of the ocular cavity (absence of disruptions in the visual field) upon completion of the job. To this end, there is a major issue that must be fulfilled, i.e. the MOFs and their respective components (metal nodes and organic linkers) must exhibit a low toxicity towards ocular tissues.

*In vitro* models based in cell cultures, instead of *in vivo* models, are the first choice to test toxicity of new compounds or nanoparticles, because of their low cost, time efficiency, their trustworthy results, and because they involve no ethical issues.<sup>38</sup>

1  
2  
3 The 661W cell line (kindly provided by Dr. Muayyad Al-Ubaidi; University of Oklahoma) is  
4 derived from retinoblastoma, a mouse retinal tumour.<sup>39</sup> This cell line expresses several markers  
5 of photoreceptor cells,<sup>40</sup> that made them one of the most widely used cell line to screen safety  
6 and efficacy in a great number of drugs for ocular treatments.<sup>41-44</sup> In fact, Januschowski et. al.  
7 suggest that cell lines derived from retinal cells such 661W or ARPE19 cells are the most  
8 accurate to evaluate retinal toxicity.<sup>45</sup> Thus, cytotoxicity of MOFs and their components was  
9 assessed in 661W cells (Figure 4). As it can be appreciated in Figure 4, except in the specific  
10 case of HKUST-1, the cell viability evaluated after 48h exposure is, in all cases, very close to  
11 100 %. These results anticipate that MIL-100 (Fe), UiO-66 and UiO-67 materials do not affect  
12 retinal photoreceptor cells viability. Only sample HKUST-1 is toxic for retinal photoreceptor  
13 cells (cell viability below 50 %), most probably due to the presence of copper and the important  
14 structural deterioration associated.

15  
16  
17  
18  
19  
20  
21  
22  
23  
24  
25  
26  
27  
28  
29  
30  
31 To confirm this point, the cytotoxicity assays have been extended to the different components  
32 of the MOF, i.e. metallic precursors and organic linkers (see Figures S8-S11). These experiments  
33 confirm that, with the exception of HKUST-1, cell viability is not affected by any of the MOF  
34 components. In addition, the effect of MIL-100 (Fe), UiO-66 and UiO-67 on cells is rather  
35 similar with different time incubations, i.e. the viability is maintained at 24h and 48h. This  
36 observation suggests that a prolonged interaction between MOFs and cells after intra-ocular  
37 injection will not be harmful for cell viability or proliferation. On the contrary, HKUST-1  
38 present time-dependent effects, as a prolonged contact with cells drops cell viability at 48h, when  
39 compared to 24h (Figures S8). An evaluation of the HKUST-1 components clearly show that the  
40 metal precursor (copper nitrate) is the one responsible for the high toxicity of the MOF.  
41  
42  
43  
44  
45  
46  
47  
48  
49  
50  
51  
52  
53  
54  
55  
56  
57  
58  
59  
60

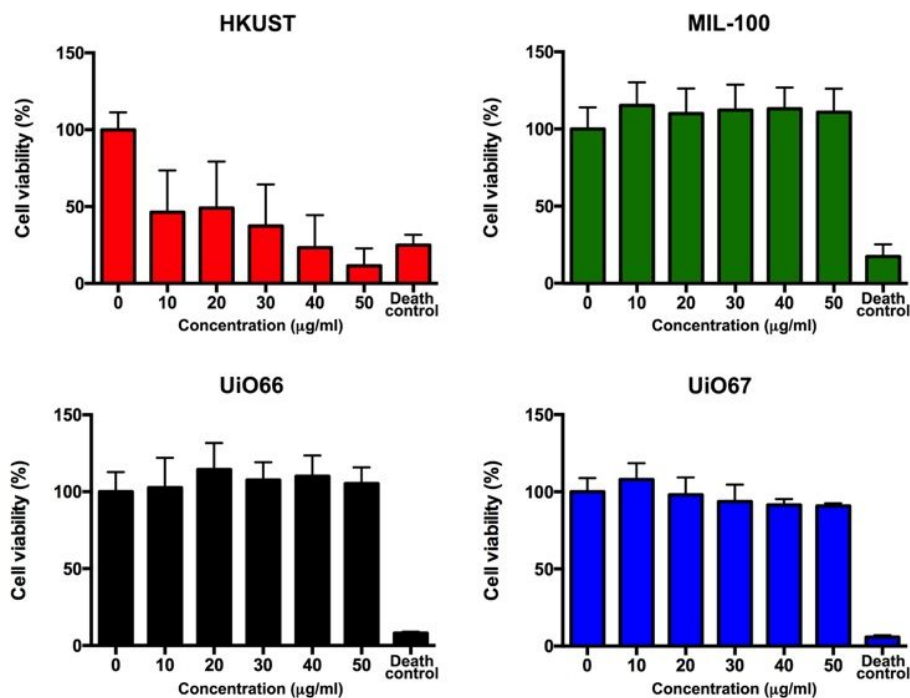


**Figure 4.** Cytotoxicity tests for the different MOFs evaluated using a retinal photoreceptor cell line (661 W) at 48h.

In summary, metal-organic frameworks can be anticipated as potential nanocarriers for drug delivery in ocular therapeutics. The proper selection of the metallic node and the organic linker allows to improve the loading capacity to values above 50 wt.%, in the specific case of UiO-67 and MIL-100 (Fe). Furthermore, the associated amorphization observed for UiO-67 in aqueous media becomes an advantage to extend the delivery kinetics up to 12 days or above. Taking into account that a patient with glaucoma requires 2-3 drops of brimonidine per day (2 mg/mL solution- ALPHAGAN), this corresponds to 0.3 mg per day or 4.5 mg every 15 days. Assuming a loading capacity for UiO-67 of 630 mg/g, patients will require the injection of 7 mg of loaded MOF every 15 days, i.e. 10 µl of MOF (considering the crystallographic density of 0.708 g/cm<sup>3</sup>).

1  
2  
3 Interestingly, these numbers are *a priori* within the theoretical threshold that human eye can  
4 hold. However, as the bioavailability of the drops is quite low (< 10%), these numbers could be  
5 even reduced for an intra-ocular administration (considering 100% bioavailability) up to 1 order  
6 of magnitude, thus validating the potential of the proposed approach.  
7  
8  
9

10  
11  
12 Furthermore, in vitro cytotoxicity results confirm the validity of our approach for drug delivery  
13 in intraocular treatments without inducing damage in photoreceptor retinal cells. These results  
14 are encouraging in terms of drug dosage and long-term delivery. However further experiments in  
15 vivo would be useful to assess the possible reaction of retinal tissue to MOFs, such as microglial  
16 activation or gliosis, due to an eventual accumulation of MOF metal nodes during long-term  
17 treatments.  
18  
19  
20  
21  
22  
23  
24  
25  
26  
27

## 28 **CONCLUSIONS**

29  
30  
31 Metal-organic frameworks (MOFs) can be anticipated as promising nanodevices for drug  
32 delivery in ocular therapeutics. Experimental results have shown that samples combining wide  
33 micropores and/or small mesopores are able to achieve a high loading capacity, above 50 wt.%  
34 (MIL-100(Fe) and UiO-67), for an alpha adrenergic receptor agonist such as brimonidine.  
35 Furthermore, delivery kinetics have shown that the associated amorphization in the case of UiO-  
36 67 upon ultrapure water or PBS exposure, as suggested by XRD measurements, can be very  
37 helpful to extends the delivery kinetic up to 12 days or above. Last but not least, cytotoxicity  
38 assays using retinal photoreceptor cells show a high biocompatibility for the MOFs evaluated,  
39 except HKUST-1, thus paving the way towards the application of MOFs in intra-ocular  
40 therapeutics.  
41  
42  
43  
44  
45  
46  
47  
48  
49  
50  
51  
52  
53  
54  
55  
56  
57  
58  
59  
60

## ASSOCIATED CONTENT

Physico-chemical characterization of the MOFs (nitrogen adsorption isotherms, F-SEM, FTIR analysis), structural stability of MOFs in aqueous solution, brimonidine tartrate loading kinetics and cytotoxicity evaluation of MOFs, linkers and metal precursors are included in the Supporting Information.

## AUTHOR INFORMATION

### Corresponding Author

\*Joaquin Silvestre-Albero; Email: [joaquin.silvestre@ua.es](mailto:joaquin.silvestre@ua.es)

### ORCID

Jesús Gandara Loe: 0000-0003-1334-4788

Isabel Ortuño Lizarán: 0000-0003-1083-9259

Laura Fernández Sánchez: 0000-0002-3629-0156

Nicolas Cuenca: 0000-0002-6767-5710

Joaquín Silvestre Albero: 0000-0002-0303-0817

### Notes

The authors declare no competing financial interest.

### Author Contributions

JGL and JSA did the preparation and characterization of the different MOFs evaluated, including the drug loading and release experiments. IOL and LFS were responsible for the cytotoxicity tests for the MOFs and the individual components. These tests were coordinated and discussed

1  
2  
3 by NC. AVE and JLA supplied the drug and participated together with JSA in the coordination  
4  
5 and discussion of this study.  
6

## 7 8 9 ACKNOWLEDGMENT

10  
11 Authors would like to acknowledge financial support from MINECO (MAT2016-80285-p),  
12  
13 GV (PROMETEOII/2014/004), H2020 (MSCA-RISE-2016/NanoMed Project). JGL  
14  
15 acknowledges GV (GRISOLIAP/2016/089) for the research contract. NC acknowledges  
16  
17 financial support from MINECO (MINECO-FEDER-BFU2015-67139-R) and GV (Prometeo  
18  
19 2016/158). IOL acknowledges Ministerio de Educación, Spain (FPU 14/03166).  
20  
21  
22  
23  
24  
25

## 26 27 REFERENCES

- 28  
29 (1) Glaucoma Research Foundation, <https://www.glaucoma.org>, accessed on September 2018.  
30  
31  
32 (2) Greenfield, D.S.; Liebmann, J.M.; Ritch, R. Brimonidine: A New Alpha2-Adrenoreceptor  
33  
34 Agonist for Glaucoma Treatment. *J. Glaucoma* **1997**, *6*, 250-258.  
35  
36  
37 (3) Beltramo, E.; Lopatina, T.; Mazzeo, A.; Arroba, A.I.; Valverde, A.M.; Hernández, C.;  
38  
39 Simó, R.; Porta, M. Effects of the Neuroprotective Drugs Somatostatin and Brimonidine on  
40  
41 Retinal Cell Models of Diabetic Retinopathy. *Acta Diabetol* 2016, *53*, 957-964.  
42  
43  
44 (4) Lambert, W.S.; Ruiz, L.; Crish, S.D.; Wheeler, L.A.; Calkins, D.J. Brimonidine Prevents  
45  
46 Axonal and Somatic Degeneration of Retinal Ganglion Cell Neurons. *Mol. Neurodegener* 2011,  
47  
48 *6*, 4.  
49  
50  
51  
52  
53  
54  
55  
56  
57  
58  
59  
60



1  
2  
3 (5) Cho, I.S.; Park, C.G.; Huh, B.K.; Cho, M.O.; Khatun, Z.; Li, Z.; Kang, S.-W.; Choy, Y.B.;  
4 Huh, K.M. Thermosensitive Hexanoyl Glycol Chitosan-based Ocular Delivery System for  
5  
6 Glaucoma Therapy. *Acta Biomater.* **2016**, *39*, 124-132.  
7  
8

9  
10 (6) Chiang, B.; Kim, Y.C.; Doty, A.C.; Grossniklaus, H.E.; Schwendeman, S.P.; Prausnitz,  
11 M.R. Sustained Reduction of Intraocular Pressure by Supraciliary Delivery of Brimonidine-  
12  
13 Loaded Poly(lactic acid) Microspheres for the Treatment of Glaucoma. *J. Controlled Release*  
14  
15 **2016**, *228*, 48-57.  
16  
17  
18

19  
20 (7) Prabhu, P.; Nitish, K.R.; Koland, M.; Harish, N.M.; Vijayanarayan, K.; Dhondge, G.;  
21 Charyulu, R.N. Preparation and Evaluation of Nano-vesicles of Brimonidine Tartrate as an  
22  
23 Ocular Drug Delivery System. *J. Young. Pharm.* **2010**, *2*, 356-361.  
24  
25  
26

27  
28 (8) Ibrahim, M.M.; Abd-Elgawad, A.-E.; Soliman, O.A.; Jablonski, M.M. Novel Topical  
29  
30 Ophthalmic Formulations for Management of Glaucoma. *Pharm. Res.* **2013**, *30*, 2818-2831.  
31  
32

33  
34 (9) Manickavasagam, D.; Wehrung, D.; Chamsaz, E.A.; Sanders, M.; Bouhenni, R.; Crish,  
35  
36 S.D.; Joy, A.; Oyewumi, M.O. Assessment of Alkoxylophenacyl-based Polycarbonates as a  
37  
38 Potential Platform for Controlled Delivery of a Model Anti-glaucoma. *Europ. J. Pharma.*  
39  
40 *Biopharma.* **2016**, *107*, 56-66.  
41  
42

43  
44 (10) Wadhwa, S.; Paliwal, R.; Paliwal, S.R.; Vyas, S.P. Nanocarriers in Ocular Drug Delivery:  
45  
46 An Update Review. *Curr. Pharm. Des.* **2009**, *15*, 2724-2750.  
47  
48

49  
50 (11) Jiang, S.; Franco, Y.L.; Zhou, Y.; Chen, J. Nanotechnology in Retinal Drug Delivery. *Int.*  
51  
52 *J. Ophthalmol.* **2018**, *11*, 1038-1044.  
53  
54  
55  
56  
57  
58  
59  
60

1  
2  
3 (12) Bachu, R.D.; Chowdhury, P.; Al-Saedi, Z.H.F.; Karla, P.K.; Boddu, S.H.S. Ocular Drug  
4 Delivery Barriers - Role of Nanocarriers in the Treatment of Anterior Segment Ocular Diseases.  
5  
6 *Pharmaceutics* **2018**, *10*, 28.  
7

8  
9  
10 (13) Li, J.; Tian, S.; Tao, Q.; Zhao, Y.; Gui, R.; Yang, F.; Zang, L.; Chen, Y.; Ping, Q.; Hou,  
11 D. Montmorillonite/Chitosan Nanoparticles as a Novel Controlled-release Topical Ophthalmic  
12 Delivery System for the Treatment of Glaucoma. *Int. J. Nanomedicine* **2018**, *13*, 3975-3987.  
13  
14

15 (14) Sun, J.; Lei, Y.; Dai, Z.; Liu, X.; Huang, T.; Wu, J.; Xu, Z.P.; Sun, X. Sustained Release  
16 of Brimonidine from a New Composite Drug Delivery System for Treatment of Glaucoma. *ACS*  
17 *Appl. Mater. Interfaces* **2017**, *9*, 7990-7999.  
18  
19

20 (15) Zhou, H.-C.; Long, J.R.; Yaghi, O.M. Introduction to Metal-Organic Frameworks. *Chem.*  
21 *Rev.* **2012**, *112*, 673-674.  
22  
23

24 (16) Horcajada, P.; Serre, C.; Vallet-Regí, M.; Sebban, M.; Taulelle, F.; Férey, G. Metal-  
25 Organic Frameworks as Efficient Materials for Drug Delivery. *Angew. Chem. Int. Ed.* **2006**, *45*,  
26 5974-5978.  
27  
28

29 (17) Horcajada, P.; Chalati, T.; Serre, C.; Gillet, B.; Sebrie, C.; Baati, T.; Eubank, J.F.;  
30 Heurtaux, D.; Clayette, P.; Kreuz, C.; Chang, J.-S.; Hwang, Y.K.; Marsaud, V.; Bories, P.-N.;  
31 Cynober, L.; Gil, S.; Férey, G.; Couvreur, P.; Gref, R. Porous Metal-Organic-Framework  
32 Nanoscale Carriers as a Potential Platform for Drug Delivery and Imaging. *Nature Mater.* **2010**,  
33 *9*, 172-178.  
34  
35

36 (18) Abuçafy, M.P.; Caetano, B.L.; Chiari-Andréo, B.G.; Fonseca-Santos, B.; do Santos, A.M.;  
37 Chorilli, M.; Chiavacci, L.A. Supramolecular Cyclodextrin-based Metal-Organic Frameworks as  
38  
39

1  
2  
3 Efficient Carrier for Anti-inflammatory Drugs. *Europ. J. Pharma. Biopharma.* **2018**, *127*, 112-  
4  
5 119.

6  
7  
8 (19) Katz, M.J.; Brown, Z.J.; Colón, Y.J.; Siu, P.W.; Scheidt, K.A.; Snurr, R.Q.; Hupp, J.T.;  
9  
10 Farha, O.K. A Facile Synthesis of UiO-66, UiO-67 and Their Derivatives. *Chem. Commun.*  
11  
12 **2013**, *49*, 9449-9451.

13  
14  
15 (20) Zhang, F.; Shi, J.; Jin, Y.; Fu, Y.; Zhong, Y.; Zhu, W. Facile Synthesis of MIL-100(Fe)  
16  
17 Under HF-free Conditions and its Application in the Acetalization of Aldehydes with Diols.  
18  
19 *Chem. Eng. J.* **2015**, *259*, 183-190.

20  
21  
22 (21) Bhagav, P.; Deshpande, P.; Pandey, S.; Chandran, S. Development and Validation of  
23  
24 Stability Indicating UV Spectrophotometric Method for the Estimation of Brimonidine Tartrate  
25  
26 in Pure Form, Formulations and Preformulation Studies. *Der Pharm. Lett.* **2010**, *2*, 106-122.

27  
28  
29 (22) Popaniya, H.S.; Patel, H.M. Simultaneous Determination of Brimonidine Tartrate and  
30  
31 Timolol Maleate in Combined Pharmaceutical Dosage form Using Two Different Green  
32  
33 Spectrophotometric Methods. *World J. Pharm. Pharm. Sci.* **2014**, *3*, 1330-1340.

34  
35  
36 (23) Toxicology Data Network, U.S. National Library of Medicine,  
37  
38 <https://toxnet.nlm.nih.gov/index.html>, accessed in September 2018.

39  
40  
41 (24) Farha, O.K.; Eryazici, I.; Jeong, N.C.; Hauser, B.G.; Wilmer, C.E.; Sarjeant, A.A.; Snurr,  
42  
43 R.Q.; Nguyen, S.T.; Yazaydin, A.Ö.; Hupp, J.T. Metal-Organic Framework Materials with  
44  
45 Ultrahigh Surface Areas: Is the Sky the Limit?. *J. Am. Chem. Soc.* **2012**, *134*, 15016-15021.  
46  
47  
48  
49  
50  
51  
52  
53  
54  
55  
56  
57  
58  
59  
60

1  
2  
3 (25) McKinstry, C.; Cussen, E.J.; Fletcher, A.J.; Patwardhan, S.V.; Sefcik, J. Scalable  
4 Continuous Production of High Quality HKUST-1 via Conventional and Microwave Heating.  
5 *Chem. Eng. J.* **2017**, *326*, 570-577.  
6  
7

8  
9  
10 (26) Tian, T.; Zeng, Z.; Vulpe, D.; Casco, M.E.; Divitini, G.; Midley, P.A.; Silvestre-Albero, J.  
11 Tan, J.-C.; Moghadam, P.Z.; Fairen-Jimenez, D. A Sol-gel Monolithic Metal-Organic  
12 Framework with Enhanced Methane Uptake. *Nature Mater.* **2018**, *17*, 174-179.  
13  
14  
15

16  
17  
18 (27) Wang, S.; Yang, Q.; Zhong, C. Adsorption and Separation of Binary Mixtures in a Metal-  
19 Organic Framework Cu-BTC: A Computational Study. *Sep. Purif. Technol.* **2008**, *60*, 30-35.  
20  
21  
22

23  
24 (28) Getzschmann, J.; Senkovska, I.; Wallacher, D.; Tovar, M.; Fairén-Jimenez, D.; Düren, T.;  
25 van Baten, J.M.; Krishna, R.; Kaskel, S. Methane Storage Mechanism in the Metal-Organic  
26 Framework Cu<sub>3</sub>(btc)<sub>2</sub>: An in Situ Neutron Diffraction Study. *Microp. Mesop. Mater.* **2010**, *136*,  
27 50-58.  
28  
29  
30  
31

32  
33  
34 (29) Lin, R.; Ge, L.; Diao, H.; Rudolph, V.; Zhu, Z. Ionic Liquid as the MOFs/Polymer  
35 Interfacial Binder for Efficient Membrane Separation. *ACS Appl. Mater. Interfaces* **2016**, *8*,  
36 32041-32049.  
37  
38  
39  
40

41  
42 (30) Tan, F.; Liu, M.; Li, K.; Wang, Y.; Wang, J.; Guo, X.; Zhang, G.; Song, C. Facile  
43 Synthesis of Size-Controlled MIL-100(Fe) with Excellent Adsorption Capacity for Methylene  
44 Blue. *Chem. Eng. J.* **2015**, *281*, 360-367.  
45  
46  
47

48  
49 (31) Leclerc, H.; Vimont, A.; Lavalley, J.-C.; Daturi, M.; Wiersum, A.D.; Llewellyn, P.L.;  
50 Horcajada, P.; Ferey, G.; Serre, C. Infrared Study of the Influence of Reducible Iron(III) Metal  
51  
52  
53

1  
2  
3 Sites on the Adsorption of CO, CO<sub>2</sub>, Propane, Propene and Propyne in the Mesoporous Metal-  
4 Organic Framework MIL-100. *Phys. Chem. Chem. Phys.* **2011**, *13*, 11748.

5  
6  
7  
8 (32) Valenzano, L.; Civalleri, B.; Chavan, S.; Bordiga, S.; Nilsen, M.H.; Jakobsen, S.; Lillerud,  
9 K.P.; Lamberti, C. Disclosing the Complex Structure of UiO-66 Metal Organic Framework: A  
10 Synergic Combination of Experiment and Theory. *Chem. Mater.* **2011**, *23*, 1700-1718.

11  
12  
13 (33) Karra, J.R.; Jasuja, H.; Huang, Y.-G.; Walton, K.S. Structural Stability of BTTB-based  
14 Metal-Organic Frameworks Under Humid Conditions. *J. Mater. Chem. A* **2015**, *3*, 1624-1631.

15  
16  
17 (34) ul Qadir, N.; Said, S.A.M.; Bahaidarah, H.M. Structural Stability of Metal Organic  
18 Frameworks in Aqueous Media - Controlling Factors and Methods to Improve Hydrostability  
19 and Hydrothermal Cyclic Stability. *Microp. Mesop. Mater.* **2015**, *201*, 61-90.

20  
21  
22 (35) Al-Janabi, N.; Hill, P.; Torrente-Murciano, L.; Garforth, A.; Gorgojo, P.; Siperstein, F.;  
23 Fan, X. Mapping the Cu-BTC Metal-Organic Framework (HKUST-1) Stability Envelope in the  
24 Presence of Water Vapour for CO<sub>2</sub> Adsorption From Flue Gases. *Chem. Eng. J.* **2015**, *281*, 669-  
25 677.

26  
27  
28 (36) Gul-E-Noor, F.; Jee, B.; Pöppel, A.; Hartmann, M.; Himsl, D.; Bertmer, M. Effects of  
29 Varying Water Adsorption on a Cu<sub>3</sub>(BTC)<sub>2</sub> Metal-Organic Framework (MOF) as Studied by <sup>1</sup>H  
30 and <sup>13</sup>C Solid-State NMR Spectroscopy. *Phys. Chem. Chem. Phys.* **2011**, *13*, 7783-7788.

31  
32  
33 (37) Orellana-Tavra, C.; Baxter, E.F.; Tian, T.; Bennett, T.D.; Slater, N.K.H.; Cheetham, A.K.;  
34 Fairen-Jimenez, D. Amorphous Metal-Organic Frameworks for Drug Delivery. *Chem. Commun.*  
35 **2015**, *51*, 13878-13881.

1  
2  
3 (38) Bakand, S. Cell Culture Techniques Essential for Toxicity Testing of Inhaled Materials  
4 and Nanomaterials In Vitro. *J. Tissue Sci. Eng.* **2016**, *7*, 1000181.  
5  
6

7  
8 (39) Bernstein, S.L.; Kutty, G.; Wiggert, B.; Albert, D.M.; Nickerson, J.M. Expression of  
9 Retina-Specific Genes by Mouse Retinoblastoma Cells. *Invest. Ophthalmol. Vis. Sci.* **1994**, *35*,  
10 3931-3937.  
11  
12  
13

14  
15 (40) Tan, E.; Ding, X.Q.; Saadi, A.; Agarwal, N.; Naash, M.I.; Al-Ubaidi, M.R. Expression of  
16 Cone-Photoreceptor-Specific Antigens in a Cell Line Derived From Retinal Tumors in  
17 Transgenic Mice. *Invest. Ophthalmol. Vis. Sci.* **2004**, *45*, 764-768.  
18  
19  
20  
21

22 (41) Chen, W.J.; Wu, C.; Kuse, Y.; Hara, H.; Duh, E.J. Nrf2 Protects Photoreceptor Cells From  
23 Photo-Oxidative Stress Induced by Blue Light. *Exp. Eye Res.* **2017**, *154*, 151-158.  
24  
25  
26  
27

28 (42) Fan, B.; Li, F.Q.; Zuo, L.; Li, G.Y. mTOR Inhibition Attenuates Glucose Deprivation-  
29 Induced Death in Photoreceptors via Suppressing a Mitochondria-Dependent Apoptotic Pathway.  
30 *Neurochem. Int.* **2016**, *99*, 178-186.  
31  
32  
33  
34

35 (43) Wyse Jackson, A.C.; Cotter, T.G. The Synthetic Progesterone Norgestrel is  
36 Neuroprotective in Stressed Photoreceptor-like Cells and Retinal Explants, Mediating its Effects  
37 via Basic Fibroblast Growth Factor, Protein Kinase A and Glycogen Synthase Kinase 3  $\beta$   
38 Signalling. *Eur. J. Neurosci.* **2016**, *43*, 899-911.  
39  
40  
41  
42  
43  
44

45 (44) Nixon, E.; Simpkins, J.W. Neuroprotective Effects of Nonfeminizing Estrogens in Retinal  
46 Photoreceptor Neurons. *Invest. Ophthalmol. Vis. Sci.* **2012**, *53*, 4739-4747.  
47  
48  
49  
50

51 (45) Januschowski, K.; Irigoyen, C.; Pastor, J.C.; Srivastava, G.K.; Romano, M.R.; Heimann,  
52 H.; Stalmans, P.; Van Keer, K.; Boden, K.; Szurman, P.; Spitzer, M.S. Retinal Toxicity of  
53  
54  
55  
56  
57  
58  
59  
60

1  
2  
3 Medical Devices Used during Vitreoretinal Surgery: A Critical Overview. *Ophthalmologica*  
4  
5 **2018**, *240*, 236-243.  
6  
7  
8  
9  
10  
11  
12  
13  
14  
15  
16  
17  
18  
19  
20  
21  
22  
23  
24  
25  
26  
27  
28  
29  
30  
31  
32  
33  
34  
35  
36  
37  
38  
39  
40  
41  
42  
43  
44  
45  
46  
47  
48  
49  
50  
51  
52  
53  
54  
55  
56  
57  
58  
59  
60